

AD-A219 861

H.H. Uhlig Corrosion Laboratory  
Massachusetts Institute of Technology

98-750

LOCALIZED CORROSION INDUCED IN  
GRAPHITE/ALUMINUM METAL-MATRIX COMPOSITES  
BY RESIDUAL MICROSTRUCTURAL CHLORIDE

AD-A219 861

DTIC  
ELECTE  
MAR 12 1980  
S B D

ADDITIONAL STATEMENT A.  
Approved for public release  
Distribution Unlimited

X0900

10U 020

2

LOCALIZED CORROSION INDUCED IN  
GRAPHITE/ALUMINUM METAL-MATRIX COMPOSITES  
BY RESIDUAL MICROSTRUCTURAL CHLORIDE

by

L.H. Hihara and R.M. Latanision

Technical Report  
to  
Office of Naval Research  
Grant No. N00014-89-J-1588

DTIC  
ELECTE  
MAR 12 1990  
S B D

Reproduction in whole or in part is  
permitted for any purpose of the  
United States Government.

The H.H. Uhlig Corrosion Laboratory  
Department of Materials Science and Engineering  
Massachusetts Institute of Technology  
Cambridge, Massachusetts 02139

February 1990-

**DISTRIBUTION STATEMENT A**  
Approved for public release;  
Distribution Unlimited

90 03 07 05 9

Unclassified

SECURITY CLASSIFICATION OF THIS PAGE

REPORT DOCUMENTATION PAGE				Form Approved OMB No. 0704-0188	
1a. REPORT SECURITY CLASSIFICATION <b>None</b>		1b. RESTRICTIVE MARKINGS			
2a. SECURITY CLASSIFICATION AUTHORITY		3. DISTRIBUTION / AVAILABILITY OF REPORT			
2b. DECLASSIFICATION / DOWNGRADING SCHEDULE					
4. PERFORMING ORGANIZATION REPORT NUMBER(S)		5. MONITORING ORGANIZATION REPORT NUMBER(S)			
6a. NAME OF PERFORMING ORGANIZATION <b>Massachusetts Institute of Technology</b>		6b. OFFICE SYMBOL <i>(if applicable)</i>	7a. NAME OF MONITORING ORGANIZATION <b>Office of Naval Research</b>		
6c. ADDRESS (City, State, and ZIP Code) <b>Room 8-202, 77 Massachusetts Avenue Cambridge, MA 02139</b>		7b. ADDRESS (City, State, and ZIP Code) <b>800 N. Quincy Street Arlington, VA 22217-5000</b>			
8a. NAME OF FUNDING / SPONSORING ORGANIZATION <b>Office of Naval Research</b>		8b. OFFICE SYMBOL <i>(if applicable)</i>	9. PROCUREMENT INSTRUMENT IDENTIFICATION NUMBER		
8c. ADDRESS (City, State, and ZIP Code) <b>Arlington, VA 22217-5000</b>		10. SOURCE OF FUNDING NUMBERS			
		PROGRAM ELEMENT NO. <b>89-J-1588</b>	PROJECT NO. <b>cor5523-02</b>	TASK NO.	WORK UNIT ACCESSION NO.
11. TITLE (Include Security Classification) <b>Localized Corrosion Induced in Graphite/Aluminum Metal-Matrix Composites by Residual Microstructural Chloride</b>					
12. PERSONAL AUTHOR(S) <b>L.H. Hihara and R.M. Latanision</b>					
13a. TYPE OF REPORT <b>Technical Report</b>		13b. TIME COVERED <b>FROM Mar 89 to 31 Dec 89</b>	14. DATE OF REPORT (Year, Month, Day) <b>February 1990</b>		15. PAGE COUNT <b>29</b>
16. SUPPLEMENTARY NOTATION <i>Aluminum</i> <i>Al</i>					
17. COSATI CODES			18. SUBJECT TERMS (Continue on reverse if necessary and identify by block number)		
FIELD	GROUP	SUB-GROUP	<b>Corrosion, metal-matrix composites, microstructural chlorides, corrosion kinetics</b>		
19. ABSTRACT (Continue on reverse if necessary and identify by block number) <b>Graphite/Al (G/Al) metal-matrix composites (MMCs) manufactured using the titanium-boron vapor deposit (Ti-B VD) method were found susceptible to localized corrosion in chloride-free sodium sulfate solutions in which Al should be passive. Corrosion behavior of G/Al MMC precursor wires and plates made of diffusion-bonded packs of precursor wires was investigated in this study. In chloride-free sodium sulfate solutions, severe pitting of the wire-wire diffusion bonds was observed to coincide with distinct pitting regimes in anodic polarization diagrams of the G/Al MMC plates. The pitting of the diffusion bond regions disbonded the precursor wires, and caused the plates to exfoliate. Pitting was found to be induced by residual microstructural chloride, which originated from the Ti-B VD method. This work suggests that the exfoliation of G/Al MMC plates should be eliminated by producing composites with halide-free microstructures.</b>					
20. DISTRIBUTION / AVAILABILITY OF ABSTRACT <input checked="" type="checkbox"/> UNCLASSIFIED/UNLIMITED <input type="checkbox"/> SAME AS RPT. <input type="checkbox"/> DTIC USERS			21. ABSTRACT SECURITY CLASSIFICATION <b>Unrestricted</b>		
22a. NAME OF RESPONSIBLE INDIVIDUAL <b>A.J. Sedriks</b>			22b. TELEPHONE (Include Area Code) <b>(202) 696-4401</b>	22c. OFFICE SYMBOL <b>1131 M</b>	

# **Localized Corrosion Induced in Graphite/Aluminum Metal-Matrix Composites by Residual Microstructural Chloride**

L.H. Hihara\* and R.M. Latanision

The H.H. Uhlig Corrosion Laboratory

Department of Materials Science and Engineering

MIT, Cambridge, MA 02139

## **Abstract**

Graphite/Al (G/Al) metal-matrix composites (MMCs) manufactured using the titanium-boron vapor deposit (Ti-B VD) method were found susceptible to localized corrosion in chloride-free sodium sulfate solutions in which Al should be passive. Corrosion behavior of G/Al MMC precursor wires and plates made of diffusion-bonded packs of precursor wires was investigated in this study. In chloride-free sodium sulfate solutions, severe pitting of the wire-wire diffusion bonds was observed to coincide with distinct pitting regimes in anodic polarization diagrams of the G/Al MMC plates. The pitting of the diffusion bond regions disbonded the precursor wires, and caused the plates to exfoliate. Pitting was found to be induced by residual microstructural chloride, which originated from the Ti-B VD method. This work suggests that the exfoliation of G/Al MMC plates should be eliminated by producing composites with halide-free microstructures.

---

\* Present address: Department of Mechanical Engineering,  
University of Hawaii at Manoa, Honolulu, Hawaii 96822

**Introduction**

Many have speculated <sup>1,2,3,4,5,6</sup> that the poor corrosion resistance of graphite/aluminum (G/Al) metal-matrix composites (MMCs) in comparison to their monolithic matrix alloys is caused by galvanic coupling of graphite and aluminum. However, the exfoliation of composite plates <sup>2,6,7</sup>, which are made of diffusion-bonded packs of G/Al MMC precursor wires and Al foils, is more destructive. Exfoliation is caused by the localized corrosion of wire-wire and wire-foil diffusion bonds (DBs), which disbonds precursor wires and foils. The cause of DB corrosion was not determined in the reported cases <sup>2,6,7</sup>.

In this study, evidence has been found that correlates localized corrosion of wire-wire DBs and occasional pitting of the matrix to residual chloride, which is left behind in the composite microstructure during fabrication. The Al-infiltration process known as the titanium-boron vapor deposit (Ti-B VD) method of manufacture, which uses  $TiCl_4$  (g) and  $BCl_3$  (g) for the deposition of a Ti-B coating on graphite fibers <sup>8</sup>, is the source of residual chloride <sup>9</sup>. The microstructure of a graphite/6061-T6 aluminum alloy (G/6061-T6 Al) MMC fabricated by the Ti-B VD method was studied in detail by Hihara and Latanision <sup>9</sup> using Auger electron spectroscopy, x-ray photoelectron spectroscopy, and energy dispersive x-ray analysis (EDXA). The results of Hihara and Latanision <sup>9</sup> will be frequently referenced, and their principal results are summarized below for convenience of the reader. Chloride contamination occurs frequently in the skin of precursor wires and occasionally in fiber-matrix interfaces. Consequently, when precursor wires are diffusion bonded in packs to produce consolidated plates, chloride-containing zones appear in DBs.

STATEMENT "A" per A.J. Sedriks  
 ONR/Code 1131M  
 TELECON

3/9/90

VG



Distribution For	
GRA&I	<input checked="" type="checkbox"/>
FAB	<input type="checkbox"/>
Unced	<input type="checkbox"/>
Location	
By <i>per telecon</i>	
Distribution/	
Availability Codes	
Dist	Avail and/or Special
<i>A-1</i>	

The corrosion of G/6061-T6 Al MMCs (processed by the Ti-B VD method) in chloride-free 0.5 M Na<sub>2</sub>SO<sub>4</sub> was investigated in this study. Since Al should passivate in chloride-free Na<sub>2</sub>SO<sub>4</sub>, pitting of the Al-matrix can be attributed to the presence of microstructural chloride. In this study, polarization diagrams were generated for monolithic 6061-T6 Al, graphite fibers, and the MMC. An optical microscope with a video recorder was used with a potentiostat and environmental cell to observe changes occurring on G/6061-T6 Al MMC electrode surfaces in situ. Scanning electron microscopy (SEM) was used to characterize corrosion morphology ex situ. This approach provided 1) electrochemical evidence which demonstrated that pitting of the 6061-T6 Al matrix in chloride-free 0.5 M Na<sub>2</sub>SO<sub>4</sub> was induced by microstructural chloride, and 2) visual evidence (in situ and ex situ) of pitting in the DB regions. Correlation between the microstructure, electrochemical data, and corrosion morphology provided firm evidence that links DB corrosion to residual microstructural chloride.

## **Materials**

### **Monolithic 6061-T6 Al Electrodes:**

Planar 6061-T6 Al electrodes were fabricated by coating specimens with either an epoxy paint (AMERCOAT 90 RESIN, Ameron) or an epoxy adhesive (EPOXY-PATCH, The Dexter Corporation). Following the coating procedure, one side of the specimens was ground flat in order to remove the epoxy from one surface to expose a planar electrode face.

### **P100 Graphite Electrodes:**

Planar graphite electrodes were fabricated from Thornel P100 fibers (which are unidirectional, continuous, about 10 μm

in diameter, and pitch-based with an elastic modulus equal to 690 GPa). Fifteen tows of the fiber (~2000 fibers/tow) were aligned unidirectionally and infiltrated with an epoxy resin (EPON 828 RESIN, Miller-Stephenson Chemical Co., Inc.). The resulting product, a graphite/epoxy composite rod, was made into electrodes by sectioning the rod perpendicularly to the axis of the fibers.

#### G/6061-T6 Al Electrodes:

G/6061 Al MMC precursor wires were produced by Material Concept, Inc. The wires consisted of a tow of Thornel P100 graphite fibers infiltrated with 6061 Al to a volume fraction of about 0.5. Six-ply plates were consolidated by DWA Composite Specialties, Inc. by diffusion bonding six layers of precursor wires between surface 6061 Al foils. The G/6061 Al MMCs were heat treated to the T6 condition by solution-treating at 530°C for 50 min, water quenching, and artificially aging at 160°C for 18 h.

Planar electrodes were made from G/6061-T6 Al MMC precursor wires and six-ply plates having the graphite fibers oriented perpendicularly to the electrode surface. The surface foils of the six-ply plate were ground away prior to making electrodes. To make electrodes, the specimens were coated with AMERCOAT 90 RESIN and then mounted in EPON 828 RESIN. Following the coating procedure, a planar electrode face was exposed, using the same method described for the 6061-T6 Al electrodes.

Precursor wires were also made into electrodes that exposed only the 6061-T6 Al skin. The tip of the precursor wires was coated with AMERCOAT 90 RESIN to shield the cross section. Consequently, when these precursor wires were

immersed into aqueous solutions, only the 6061-T6 Al skin was exposed. These electrodes will be referred to as precursor-wire 6061-T6 Al skin electrodes.

#### **Aqueous Solutions:**

Neutral 0.5 M Na<sub>2</sub>SO<sub>4</sub> and 3.15 wt% NaCl solutions were prepared from 18 megaohm-cm water, and analytical grade Na<sub>2</sub>SO<sub>4</sub> (< 0.0002% Cl) and NaCl, respectively. During potentiodynamic experiments, the solutions were kept at 30 ± 0.1°C, and deaerated with pre-purified hydrogen or aerated with 19.5 to 23.5 % oxygen balanced with nitrogen. In experiments performed under the optical microscope, solutions were at room temperature and exposed to laboratory air. Gas pressure was 1 atm.

#### **Instrumentation and Procedure**

##### **Electrochemical Experimentation**

The surface of all planar electrodes was polished to a 0.05 µm finish with gamma alumina powder, kept wet, and rinsed with 18 megaohm-cm water about 5 minutes prior to immersion in the aqueous solutions. The precursor-wire 6061-T6 Al skin electrodes were rinsed in methanol and then in 18 megaohm-cm water about 5 minutes before immersion in the aqueous solutions.

Potentiodynamic polarization examinations were conducted with a Model 173 Princeton Applied Research (PAR) Potentiostat/Galvanostat and a Model 376 PAR Logarithmic Current Converter. The accuracy of the logarithmic current converter was measured to be better than 5% while measuring currents in the nA range.

In generating potentiodynamic polarization diagrams, the electrodes were allowed to stabilize at their corrosion potentials ( $E_{\text{corr}}$ ) and were subsequently polarized at a rate of 0.1 mV/s. Polarization diagrams with error bars were generated from at least three individual polarization diagrams. The average logarithm of the current density ( $\log i$  [A/cm<sup>2</sup>]) was plotted as a function of potential. The peak-to-peak width between error bars is equal to two times the standard deviation of  $\log i$ . The average values of  $E_{\text{corr}}$ , the average time that the electrodes were in the open circuit condition prior to polarization, and the standard deviation (SD) of these parameters are given in the caption of the polarization diagrams.

### Corrosion Morphology

Optical microscopy and SEM were used to characterize the corrosion morphology. Chemical analysis of solid corrosion products was performed by EDXA.

In situ corrosion observations were made using an optical microscope equipped with a video camera and recorder. An open cell contained the solution and held the specimen beneath the objective lens of the microscope. There were several millimeters of solution above the specimen surface.

## **Results**

### Electrochemical Data

In order to recognize peculiarities in the electrochemical behavior of the G/6061-T6 Al MMC plate (exposed to 0.5 M Na<sub>2</sub>SO<sub>4</sub>), the anodic polarization diagram of the actual composite was compared to that of a multiple electrode model.

The model represented "ideal" behavior. Accordingly, anodic polarization diagrams of monolithic 6061-T6 Al, P100 graphite fiber, and G/6061-T6 Al MMCs were generated. Because residual microstructural chloride is expected to induce pitting in the 6061-T6 Al matrix, it is important to know how chloride affects the anodic polarization diagram of 6061-T6 Al. For this reason, an anodic polarization diagram of monolithic 6061-T6 Al exposed to 3.15 wt% NaCl was generated.

#### Monolithic 6061-T6 Al:

Anodic polarization diagrams of 6061-T6 Al are shown in Figures 1 (deaerated 0.5 M Na<sub>2</sub>SO<sub>4</sub>) and 2 (deaerated 3.15 wt% NaCl). The 6061-T6 Al passivated in the Na<sub>2</sub>SO<sub>4</sub> solution, and pitted in the NaCl solution (pitting potential = -0.725 V<sub>SCE</sub>).

#### P100 Graphite Fiber:

The anodic polarization diagram of P100 graphite fiber exposed to deaerated 0.5 M Na<sub>2</sub>SO<sub>4</sub> is shown in Figure 1.

#### G/6061-T6 Al MMC:

Anodic polarization diagrams of planar six-ply plate (Figures 3) and precursor wire (Figure 4) that were exposed to deaerated 0.5 M Na<sub>2</sub>SO<sub>4</sub> are similar, with pitting potentials at approximately -0.5 V<sub>SCE</sub>. The open circuit potential of planar six-ply plate electrodes was shifted in the noble direction towards the pitting potential during aeration, as shown in Figure 5. The anodic polarization diagram of the precursor-wire 6061-T6 Al skin electrode (Figure 6) exposed to deaerated 0.5 M Na<sub>2</sub>SO<sub>4</sub> is also similar to Figures 3 and 4; the pitting potential of the precursor-wire skin was about -0.6 V<sub>SCE</sub>.

## Corrosion Morphology

In chloride-free 0.5 M Na<sub>2</sub>SO<sub>4</sub>, the matrix of the G/6061-T6 Al MMC pitted in the zones of residual microstructural chloride. Of the various types of electrodes examined, the zones were located in 1) the DB regions of the planar six-ply plate electrodes, 2) the perimeter regions of the planar precursor wire electrodes, and 3) the skin of the precursor-wire 6061-T6 Al skin electrodes. The graphite fibers were relatively inert, but could be oxidized at noble potentials.

### Planar Six-ply Plate Electrodes:

The corrosion process was observed in situ with an optical microscope, and can be viewed on video tape elsewhere <sup>10</sup>. Hydrogen evolution was observed in the DB regions during exposure to aerated 0.5 M Na<sub>2</sub>SO<sub>4</sub> in the open circuit condition (-0.61 V<sub>SCE</sub>). Dissolution of the DB regions was intensified by anodic polarization, and the resulting corrosion morphology is shown in Figure 7. The disbonding of precursor wires by corrosion was demonstrated by sawing off the surface layer from a corroded electrode, similar to that in Figure 7, to produce a wafer which could then be slightly stressed in tension. Following this procedure, the wafer parted along thoroughly-corroded DBs (Figure 8); the corrosion product in the region contained chlorine, as determined by EDXA. Occasionally, pits were also found in precursor interiors, as shown in Figure 9.

### Planar Precursor Wire Electrodes:

Pits were concentrated near the perimeter of planar precursor-wire electrodes (Figure 10) that were anodically polarized in 0.5 M Na<sub>2</sub>SO<sub>4</sub>. With the optical microscope, H<sub>2</sub> evolution was also seen in the perimeter regions during

anodic polarization (at 0.0  $V_{SCE}$ ). In this case,  $H_2$  evolution is an indication of pitting because the reducing potentials within pits can promote  $H_2$  evolution.

#### **Precursor-wire 6061-T6 Al Skin Electrodes:**

Pits were copious in the skin of precursor-wire 6061-T6 Al skin electrodes (Figure 11) that were anodically polarized in deaerated 0.5 M  $Na_2SO_4$ . Beneath the skin, dissolution of the matrix was extensive, as shown by a cross-sectional slice (Figure 12). An enlargement of the cross section shows sites where pits penetrated the skin (Figure 13). In Figures 12 and 13, the large cavities (black) resulted from mechanical damage during sectioning.

#### **Graphite Fiber in G/6061-T6 Al MMC:**

Figure 14 shows crevices that formed along perimeters of graphite fibers during anodic polarization at 2.0  $V_{SCE}$  for 3.2 hours at 30°C in deaerated 0.5 M  $Na_2SO_4$ .

#### **Discussion**

The electrochemical evidence of pitting in chloride-free 0.5 M  $Na_2SO_4$ , and the localized corrosion of DB regions are two principal findings presented in the Results section. These results in concert with those of Hihara and Latanision<sup>9</sup>, which revealed that chloride-containing zones are located in DB regions, provide sufficient evidence to link DB corrosion to residual microstructural chloride. The following discussion establishes that 1) pitting was induced by residual chloride, as revealed by a comparison of the electrochemical behavior of the multiple electrode model to that of the actual MMC, 2) corrosion morphology was related to the microstructure, 3) DB corrosion in the open circuit condition was caused by  $O_2$  reduction, and

4) crevice formation, which occurs along the perimeters of P100 graphite fibers, was caused by graphite oxidation and not by fiber-matrix interfacial dissolution.

The multiple electrode model for a composite containing 50% P100 graphite fibers and 6061-T6 Al exposed to deaerated 0.5 M Na<sub>2</sub>SO<sub>4</sub> is shown in Figure 1. In the multiple electrode model, 6061-T6 Al was passive, and P100 graphite was oxidized primarily to CO<sub>2</sub>. Hihara <sup>10</sup> showed that significant amounts of CO<sub>2</sub> are liberated from P100 graphite anodes during polarization in 0.5 M Na<sub>2</sub>SO<sub>4</sub>. In Figure 15, the polarization diagram of the multiple electrode model is compared to the actual diagram of the G/6061-T6 Al MMC six-ply plate. The pitting regime in the polarization diagram of the six-ply plate (Figure 3 or 15) caused current densities to be much larger than predicted by the multiple electrode model. In fact, pitting regimes were found in all of the anodic polarization diagrams of the various G/6061-T6 Al electrodes exposed to chloride-free 0.5 M Na<sub>2</sub>SO<sub>4</sub>. This can be seen in Figures 4 and 6, showing the anodic polarization diagrams of the planar precursor wire and precursor-wire 6061-T6 Al skin electrodes, respectively. It is evident that microstructural chloride induces pitting of 6061-T6 Al in much the same manner as would Cl<sup>-</sup> ions originating from solution. This was further demonstrated by comparing the anodic polarization diagram of the precursor-wire 6061-T6 Al skin electrode exposed to chloride-free 0.5 M Na<sub>2</sub>SO<sub>4</sub> to that of monolithic 6061-T6 Al exposed to 3.15 wt% NaCl (Figure 16). Although there is a difference in the pitting potentials by about 0.1 V (Figure 16), the difference was anticipated due to the dependency of pitting potentials on chloride-ion concentration <sup>11</sup>.

The corrosion morphology also provided firm evidence that links localized corrosion to microstructural chloride. High pit density corresponded to the zones of microstructural chloride. In the planar electrodes, the zones were located in the DB regions of six-ply plates, and in the perimeter of precursor wires. In the precursor-wire 6061-T6 Al skin electrodes, the zone encompassed the skin<sup>9</sup>. Accordingly, in the planar electrodes, severe pitting occurred in the DB regions of six-ply plates (Figures 7 and 8) and in the perimeter regions of precursor wires (Figure 10). In the precursor-wire skin electrode, the skin severely pitted (Figures 11, 12, and 13). Also, the corrosion of DB regions led to the disbonding of precursor wires in the six-ply plate electrodes. It is likely that this type of disbonding resulted in the exfoliation of G/Al plates that were seen by others<sup>2,6,7</sup>. An important implication is that composites with halide-free DBs should not exfoliate.

In the six-ply plates, pitting of the matrix also occurred in precursor-wire interiors, as shown in Figure 9. Pitting in the precursor interiors, which occurred infrequently in comparison to pitting in the DB regions, is probably induced by chloride contamination of fiber-matrix interfaces, which is also infrequent<sup>9</sup>.

It is also important to know if pitting occurs in the open circuit condition, which is likely to be the case during service conditions. In deaerated 0.5 M Na<sub>2</sub>SO<sub>4</sub>, the polarization diagrams (Figures 3, 4, and 6) show that G/6061-T6 Al MMCs were spontaneously passive. In aerated solutions, however, a planar six-ply plate electrode (exposed to 0.5 M Na<sub>2</sub>SO<sub>4</sub>) was polarized into the vicinity of the pitting regime by O<sub>2</sub> reduction. This is shown in Figure 5 where the open circuit potential

approaches the pitting potential. Hydrogen evolution was also observed (in situ with an optical microscope) in the DB regions of newly polished six-ply plate exposed to aerated 0.5 M Na<sub>2</sub>SO<sub>4</sub> in the open circuit condition (-0.61 V<sub>sce</sub>). H<sub>2</sub> evolution, in this case, is a sign of pitting because potentials within pits can be sufficiently reducing to promote H<sub>2</sub> evolution. It is doubtful that methane evolution resulting from Al<sub>4</sub>C<sub>3</sub> hydrolysis or graphite reduction can occur at DB regions. Al<sub>4</sub>C<sub>3</sub> should be localized in fiber-matrix interfaces and not in DBs because it is a reaction product of graphite and Al at high processing temperatures. Methane, which is thermodynamically stable at cathodic potentials, was undetectable during cathodic polarization of P100 graphite fiber electrodes in 0.5 M Na<sub>2</sub>SO<sub>4</sub><sup>10</sup>.

Finally, comments are due regarding crevices that formed along fiber perimeters (Figure 14) which could be mistaken for dissolution of fiber-matrix interfaces. The crevices formed during anodic polarization in 0.5 M Na<sub>2</sub>SO<sub>4</sub>. The corrosion morphology shown in Figure 14 is identical to that seen in graphite/epoxy composites<sup>10</sup>. Epoxy is unaffected by anodic polarization whereas the graphite fibers are oxidized primarily to CO<sub>2</sub><sup>10</sup>. Since the Al matrix in G/6061-T6 Al MMCs should passivate near fiber-matrix interfaces (where microstructural chloride is rarely found<sup>9</sup>), the corrosion morphology is expected to be similar to that of graphite/epoxy composites. Thus, the apparent interfacial dissolution was actually the result of graphite oxidation.

### **Conclusion**

Chloride-containing zones in DBs of G/6061-T6 Al MMC plates were found to cause severe pitting in DB regions. The pitting of DB regions disbonds precursor wires, which leads to

the exfoliation of six-ply plate electrodes. Exfoliation is much more destructive than classical galvanic corrosion between graphite and Al. This work suggests that exfoliation can be eliminated from future G/Al MMCs by producing composites with halide-free DBs. In view of these findings, priority should be given to fabrication processes that do not use halides.

### **Acknowledgements**

We are grateful for the financial support provided by the Shell Companies Foundation and the Office of Naval Research (grant # N00014-89-J-1588). We are particularly grateful to Dr. S.G. Fishman of the Office of Naval Research, and to Dr. W.C. Harrigan, Jr. of DWA Composite Specialties, Inc.

### **References**

- 1) W.F. Czyrklis, Corrosion/85, Paper No. 196, NACE, Houston, Texas, 1985.
- 2) M.G. Vassilaros, D.A. Davis, G.L. Steckel, J.P. Gudas, in Mechanical Behavior of Metal-Matrix Composites, Ed. J.E. Hack, M.F. Amateau, The Metallurgical Society of the AIME, 1983, p.335.
- 3) D.L. Dull, W.C. Harrigan, Jr., M.F. Amateau, Aerospace Corporation, AD - A011 761, 1975.
- 4) J.M. Evans, D.M. Braddick, Corros. Sci., Vol.11, 1971, p.611.
- 5) E.G. Kendall, D.L. Dull, "Salt Water Corrosion Behavior of Aluminum-Graphite Composite," National Technical Information Service, U.S. Department of Commerce, AD-777 160, 1974.
- 6) D.M. Aylor, R.M. Kain, in Recent Advances in Composites in the United States and Japan, Ed. J.R. Vinson, M. Taya, ASTM Special Technical Publication 864, 1983, p.632.

- 7) W.H. Pfeifer, in Hybrid and Select Metal-Matrix Composites, Ed. W.J. Renton, American Institute of Aeronautics and Astronautics, 1977, p.231.
- 8) W.C. Harrigan, Jr., R.H. Flowers, in Failure Modes in Composites IV, Ed. J.A. Cornie, F.W. Crossman, The Metallurgical Society of AIME, 1977, p.319.
- 9) L.H. Hihara, R.M. Latanision, Mater. Sci. E. A, in Press.
- 10) L.H. Hihara, "Corrosion of Aluminum-Matrix Composites," Ph.D. Thesis, Massachusetts Institute of Technology, 1989.
- 11) J.R. Galvele, in Passivity of Metals, Ed. R.P. Frankenthal, J. Kruger, The Electrochemical Society, Inc. 1978, p.285.

### List of Figures

Figure 1: Anodic polarization diagrams of 6061-T6 Al and P100 graphite fiber exposed to deaerated 0.5 M Na<sub>2</sub>SO<sub>4</sub> of pH 7 at 30°C. Scan rate = 0.1 mV/s. Based on the mixed electrode theory, these diagrams were used to construct the anodic polarization diagram of a composite consisting of 50% P100 graphite fiber and 6061-T6 Al. Data for 6061-T6 Al: Avg  $E_{CORR}$  = -1.256 V<sub>SCE</sub>, SD = 0.010 V; Avg time at open circuit = 0.59 h, SD = 0.09 h. Data for P100 graphite fiber: Avg  $E_{CORR}$  = -0.190 V<sub>SCE</sub>, SD = 0.64 V; Avg time at open circuit = 2.21 h, SD = 1.11 h.

Figure 2: Anodic polarization diagram of 6061-T6 Al exposed to deaerated 3.15 wt% NaCl of pH 7 at 30°C. Scan rate = 0.1 mV/s; Avg  $E_{CORR}$  = -1.228 V<sub>SCE</sub>, SD = 0.029 V; Avg time at open circuit = 0.67 h, SD = 0.18 h.

Figure 3: Anodic polarization diagram of planar G/6061-T6 Al MMC six-ply plate electrode exposed to deaerated 0.5 M Na<sub>2</sub>SO<sub>4</sub> of pH 7 at 30°C. Scan rate = 0.1 mV/s; Avg E<sub>CORR</sub> = -0.915 V<sub>SCE</sub>, SD = 0.018 V; Avg time at open circuit = 0.93 h, SD = 0.17 h.

Figure 4: Anodic polarization diagram of planar G/6061-T6 Al MMC precursor wire electrode exposed to deaerated 0.5 M Na<sub>2</sub>SO<sub>4</sub> of pH 7 at 30°C. Scan rate = 0.1 mV/s; Avg E<sub>CORR</sub> = -1.050 V<sub>SCE</sub>, SD = 0.005 V; Avg time at open circuit = 0.62 h, SD = 0.03 h.

Figure 5: Anodic polarization diagram of planar G/6061-T6 Al MMC six-ply plate electrode exposed to aerated 0.5 M Na<sub>2</sub>SO<sub>4</sub> of pH 7 at 30°C. Scan rate = 0.1 mV/s; Avg E<sub>CORR</sub> = -0.680 V<sub>SCE</sub>, SD = 0.048 V; Avg time at open circuit = 1.55 h, SD = 0.57 h.

Figure 6: Anodic polarization diagram of precursor-wire 6061-T6 Al skin electrode exposed to deaerated 0.5 M Na<sub>2</sub>SO<sub>4</sub> of pH 7 at 30°C. Scan rate = 0.1 mV/s; Avg E<sub>CORR</sub> = -1.081 V<sub>SCE</sub>, SD = 0.017 V; Avg time at open circuit = 0.71 h, SD = 0.08 h.

Figure 7: SEM micrograph showing the localized dissolution (induced by residual microstructural chloride) of the diffusion bond regions between precursor wires in a planar G/6061-T6 Al MMC six-ply plate electrode. The electrode was anodically polarized in deaerated 0.5 M Na<sub>2</sub>SO<sub>4</sub> of pH 7 at 30°C.

Figure 8: SEM micrograph of a planar G/6061-T6 Al MMC six-plate electrode showing the disbonding of precursor wires resulting from localized dissolution (induced by residual microstructural chloride) of the diffusion bond regions. The electrode was anodically polarized in deaerated 0.5 M Na<sub>2</sub>SO<sub>4</sub> of pH 7 at 30°C.

Figure 9: SEM micrograph of a planar G/6061-T6 Al MMC six-plate electrode showing localized dissolution (induced by residual microstructural chloride) in precursor interiors. Graphite fibers (dark) are in a 6061-T6 Al matrix (light). The electrode was anodically polarized in deaerated 0.5 M Na<sub>2</sub>SO<sub>4</sub> of pH 7 at 30°C.

Figure 10: SEM micrograph showing localized dissolution (induced by residual microstructural chloride) in the perimeter region (indicated by arrows) of a planar G/6061-T6 Al MMC precursor wire electrode. The graphite fibers (dark) are in a 6061-T6 Al matrix (light). The precursor wire is mounted in epoxy. The electrode was anodically polarized in deaerated 0.5 M Na<sub>2</sub>SO<sub>4</sub> of pH 7 at 30°C.

Figure 11: SEM micrograph showing pits (induced by residual microstructural chloride) in a precursor-wire skin electrode. The electrode was anodically polarized in deaerated 0.5 M Na<sub>2</sub>SO<sub>4</sub> of pH 7 at 30°C.

Figure 12: Cross section of the precursor-wire 6061-T6 Al skin electrode shown in Figure 11. The graphite fibers (dots) are perpendicular to the plane of the page. The bright regions are unconsumed 6061-T6 Al matrix. The electrode was anodically polarized in deaerated 0.5 M Na<sub>2</sub>SO<sub>4</sub> of pH 7 at 30°C.

Figure 13: Enlarged view of Figure 12 showing sites where pits (indicated by arrows) initially penetrated the precursor-wire skin.

Figure 14: SEM micrograph showing crevices along the perimeters of graphite fibers in a planar G/6061-T6 Al MMC six-ply plate electrode that was anodically polarized at 2.0 V<sub>SCE</sub> for 3.2 h in deaerated 0.5 M Na<sub>2</sub>SO<sub>4</sub> of pH 7 at 30°C. The formation of crevices was caused by CO<sub>2</sub> evolution, resulting from the oxidation of graphite.

Figure 15: Comparison of the anodic polarization diagram of the multiple electrode model (consisting of 50% P100 graphite fiber and 6061-T6 Al) to that of the planar G/6061-T6 Al MMC (~50 vol % P100 graphite) six-ply plate electrode exposed to deaerated 0.5 M Na<sub>2</sub>SO<sub>4</sub> of pH 7 at 30°C. Scan rate = 0.1 mV/s.

Figure 16: Comparison of the anodic polarization diagram of the precursor-wire 6061-T6 Al skin electrode exposed to deaerated chloride-free 0.5 M Na<sub>2</sub>SO<sub>4</sub> to that of monolithic 6061-T6 Al exposed to deaerated 3.15 wt% NaCl. Both solutions were of pH 7 at 30°C. Scan rate = 0.1 mV/s.

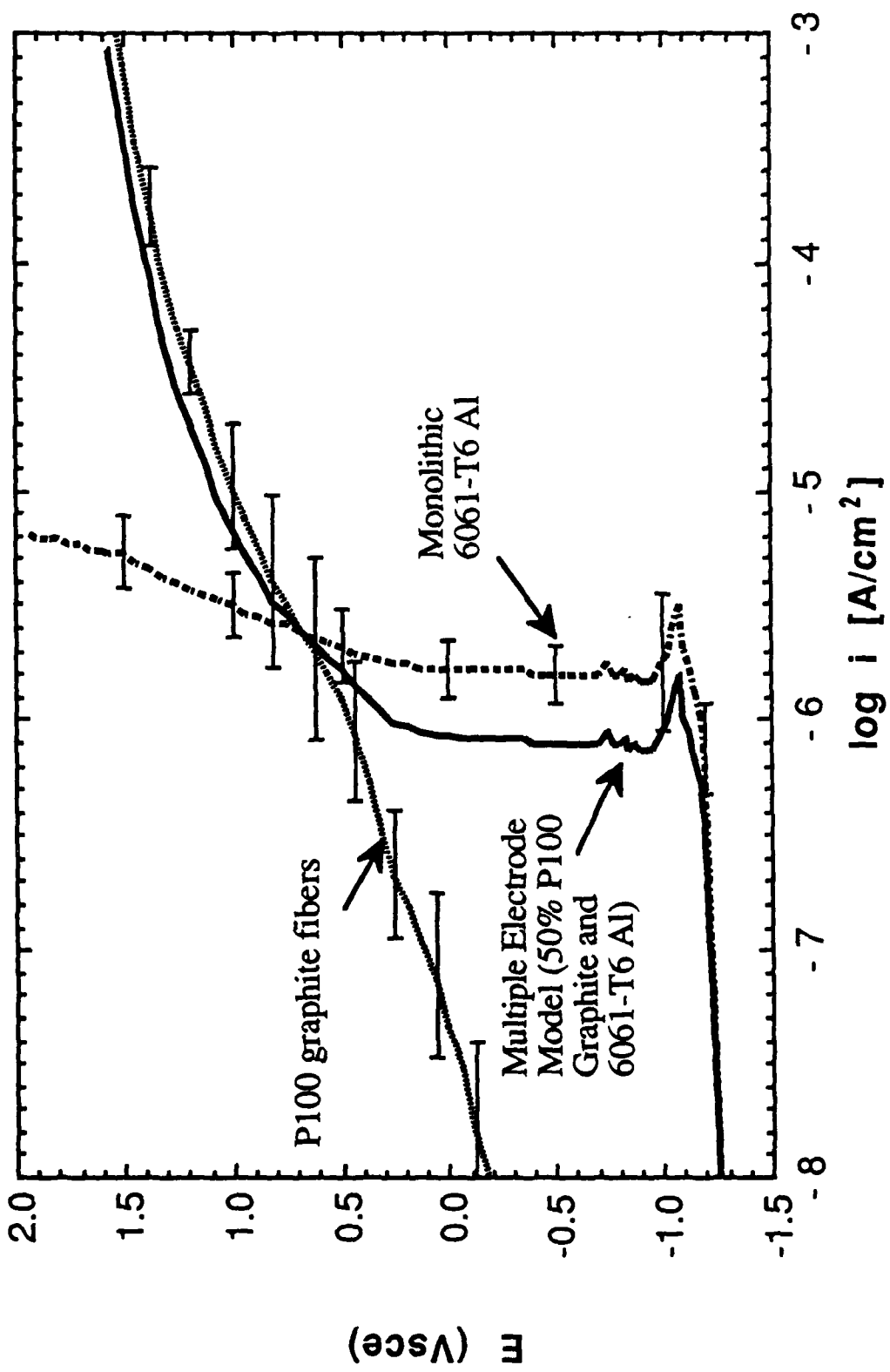


Figure 1: Anodic polarization diagrams of 6061-T6 Al and P100 graphite fiber exposed to deaerated 0.5 M Na<sub>2</sub>SO<sub>4</sub> of pH 7 at 30°C. Scan rate = 0.1 mV/s. Based on the mixed electrode theory, these diagrams were used to construct the anodic polarization diagram of a composite consisting of 50% P100 graphite fiber and 6061-T6 Al. Data for 6061-T6 Al: Avg  $E_{\text{corr}} = -1.256 \text{ V}_{\text{SCE}}$ , SD = 0.010 V; Avg time at open circuit = 0.59 h, SD = 0.09 h. Data for P100 graphite fiber: Avg  $E_{\text{corr}} = -0.190 \text{ V}_{\text{SCE}}$ , SD = 0.64 V; Avg time at open circuit = 2.21 h, SD = 1.11 h.

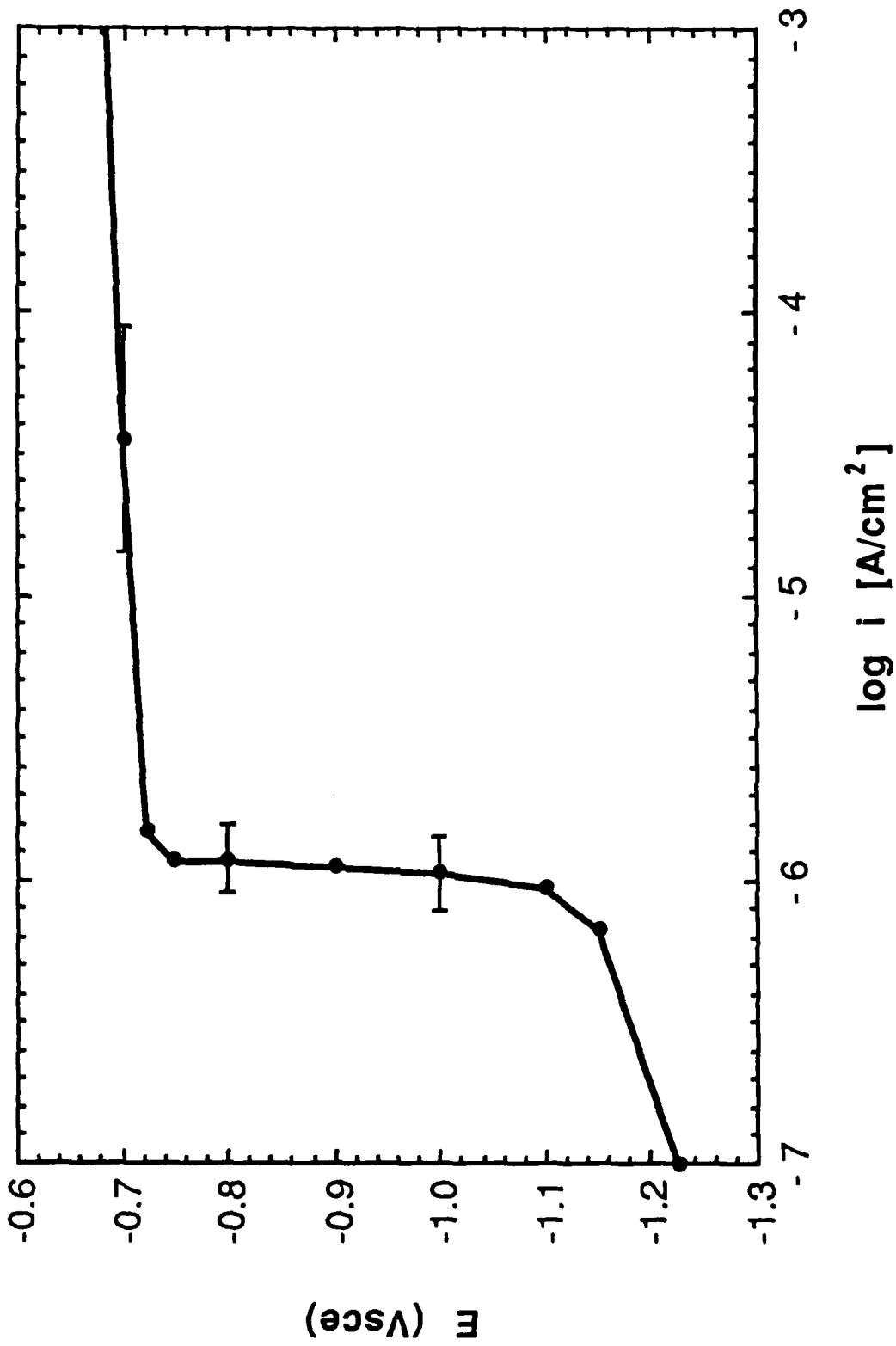


Figure 2: Anodic polarization diagram of 6061-T6 Al exposed to deaerated 3.15 wt% NaCl of pH 7 at 30°C. Scan rate = 0.1 mV/s; Avg  $E_{\text{CORR}} = -1.228$  V<sub>SCE</sub>, SD = 0.029 V; Avg time at open circuit = 0.67 h, SD = 0.18 h.

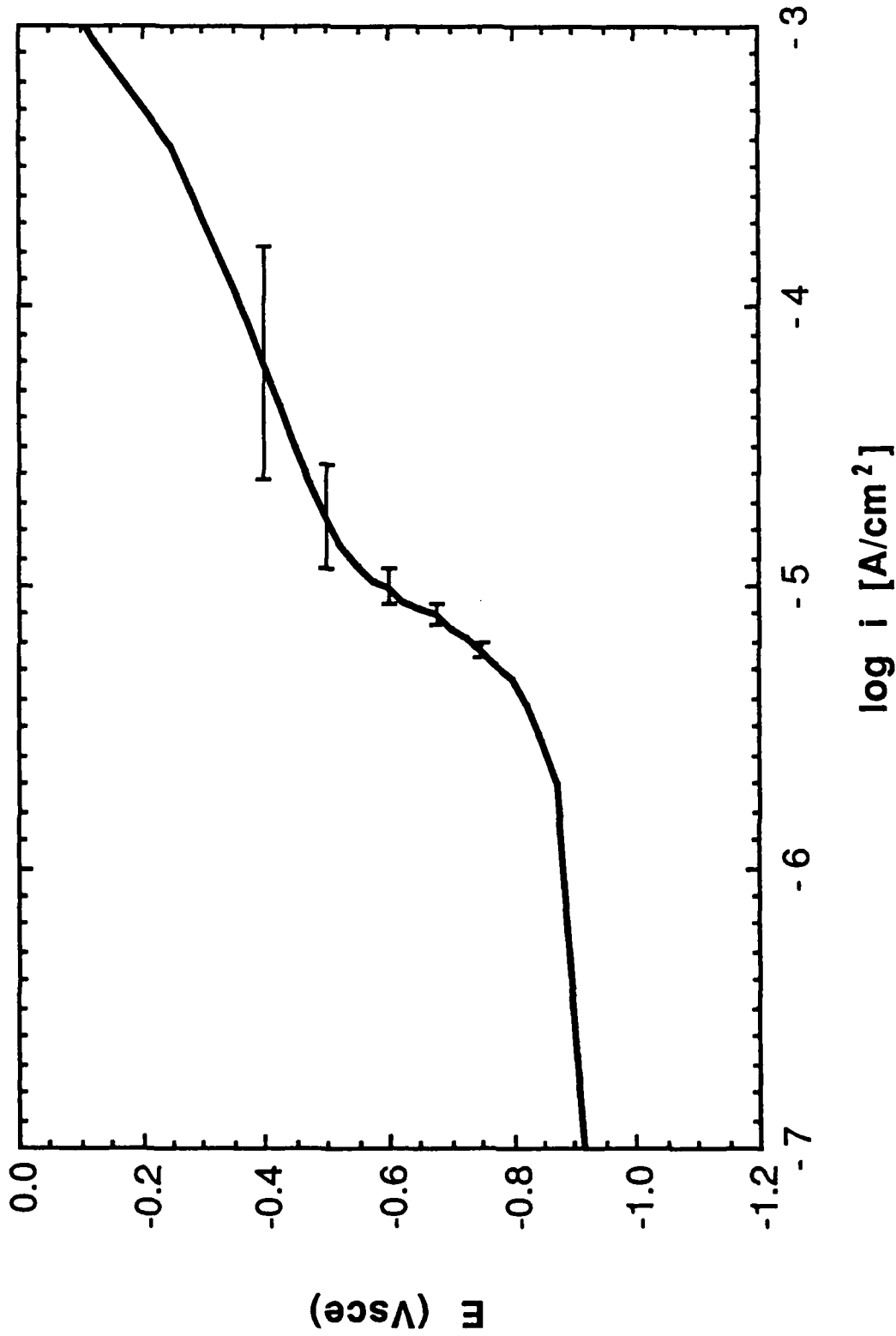


Figure 3: Anodic polarization diagram of planar G/6061-T6 Al MMC six-ply plate electrode exposed to deaerated 0.5 M Na<sub>2</sub>SO<sub>4</sub> of pH 7 at 30°C. Scan rate = 0.1 mV/s; Avg  $E_{\text{corr}} = -0.915$  V<sub>sce</sub>; SD = 0.018 V; Avg time at open circuit = 0.93 h, SD = 0.17 h.

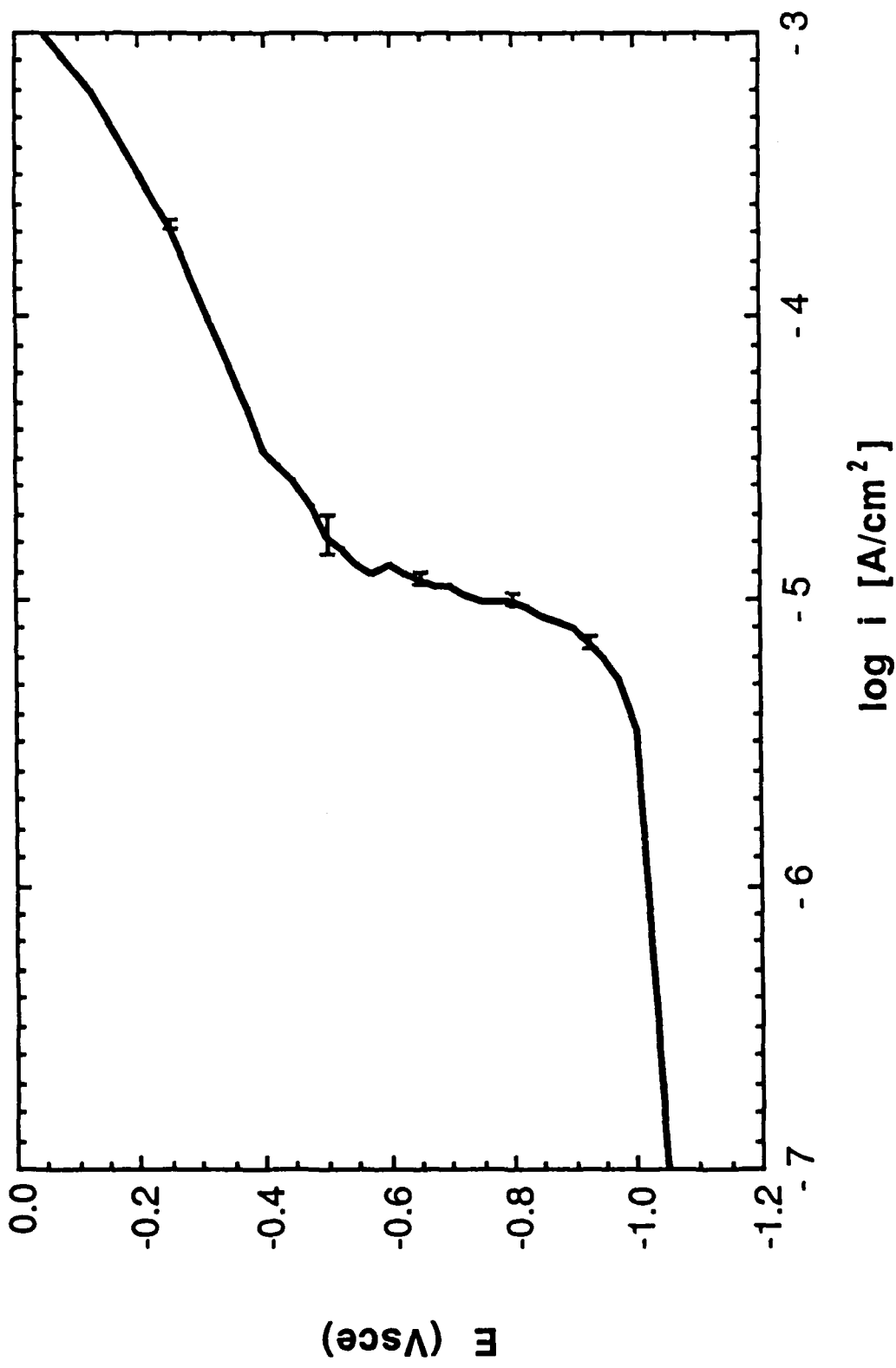


Figure 4: Anodic polarization diagram of planar G/6061-T6 Al MMC precursor wire electrode exposed to deaerated 0.5 M Na<sub>2</sub>SO<sub>4</sub> of pH 7 at 30°C. Scan rate = 0.1 mV/s; Avg E<sub>corr</sub> = -1.050 V<sub>sce</sub>; SD = 0.005 V; Avg time at open circuit = 0.62 h, SD = 0.03 h.

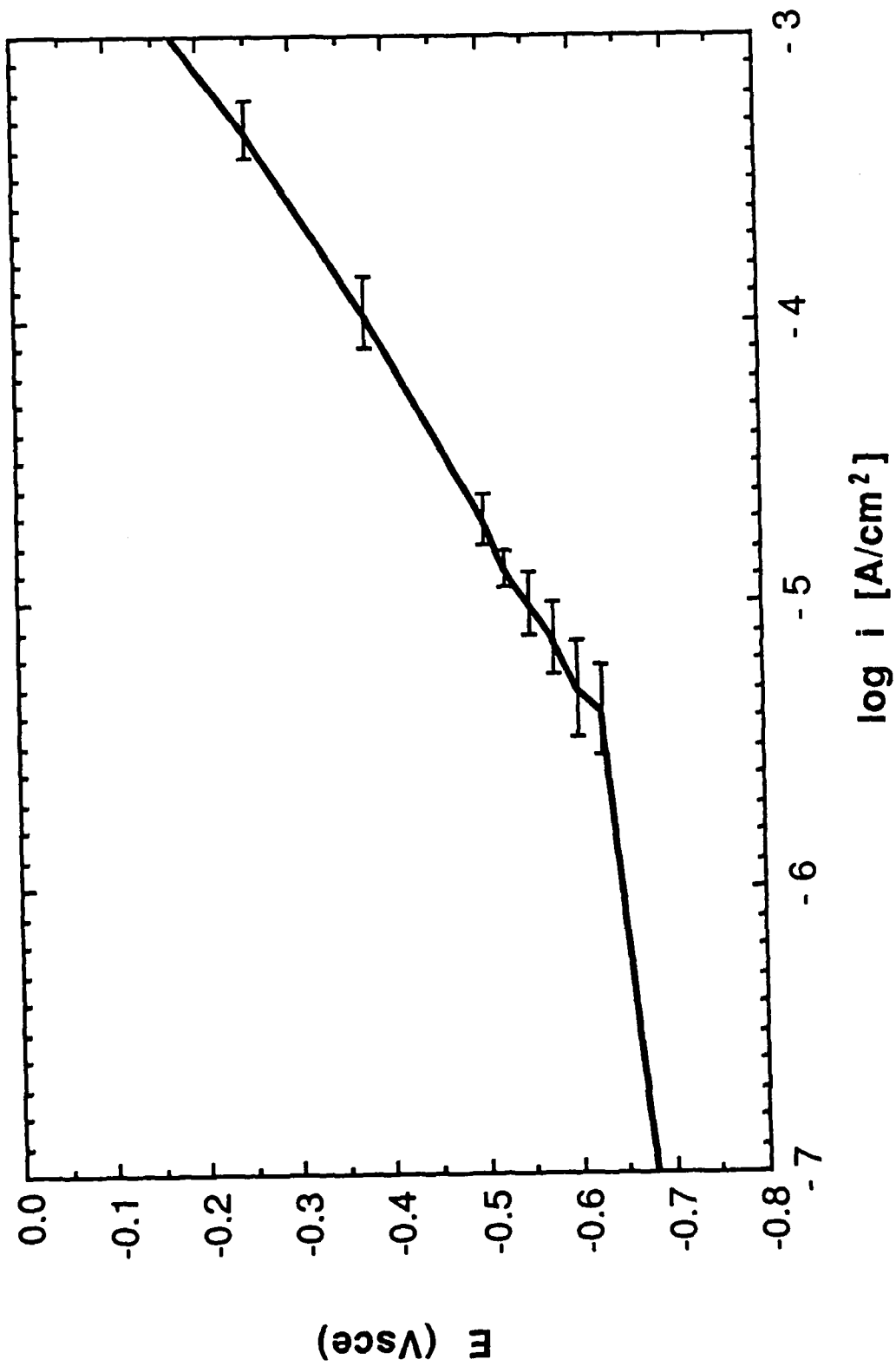


Figure 5: Anodic polarization diagram of planar G/6061-T6 Al MMC six-ply plate electrode exposed to aerated 0.5 M Na<sub>2</sub>SO<sub>4</sub> of pH 7 at 30°C. Scan rate = 0.1 mV/s; Avg  $E_{\text{corr}} = -0.680$  V<sub>sce</sub>; SD = 0.048 V; Avg time at open circuit = 1.55 h, SD = 0.57 h.

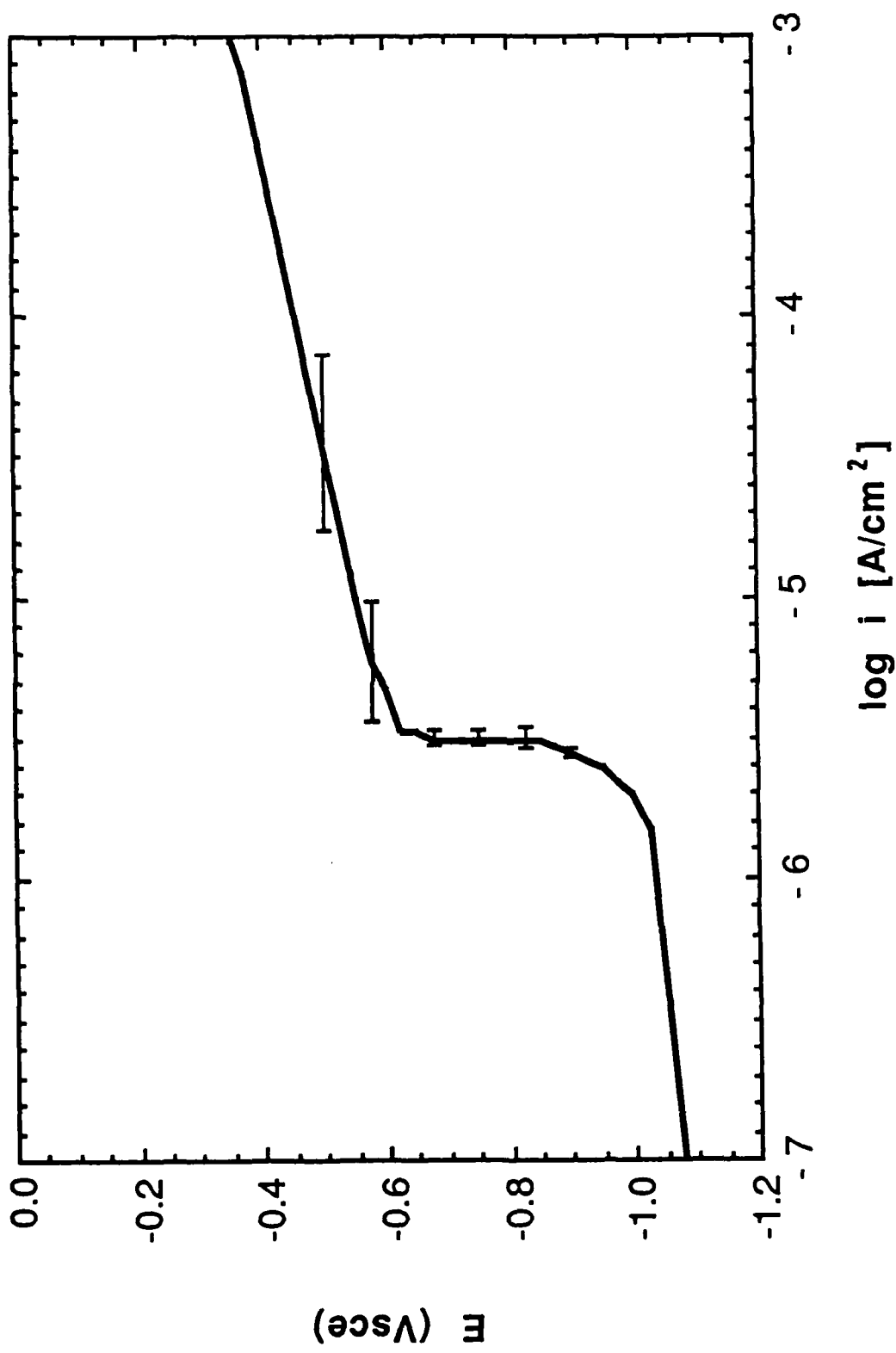


Figure 6: Anodic polarization diagram of precursor-wire 6061-T6 Al skin electrode exposed to deaerated 0.5 M Na<sub>2</sub>SO<sub>4</sub> of pH 7 at 30°C. Scan rate = 0.1 mV/s; Avg E<sub>corr</sub> = -1.081 V<sub>sce</sub>, SD = 0.017 V; Avg time at open circuit = 0.71 h, SD = 0.08 h.

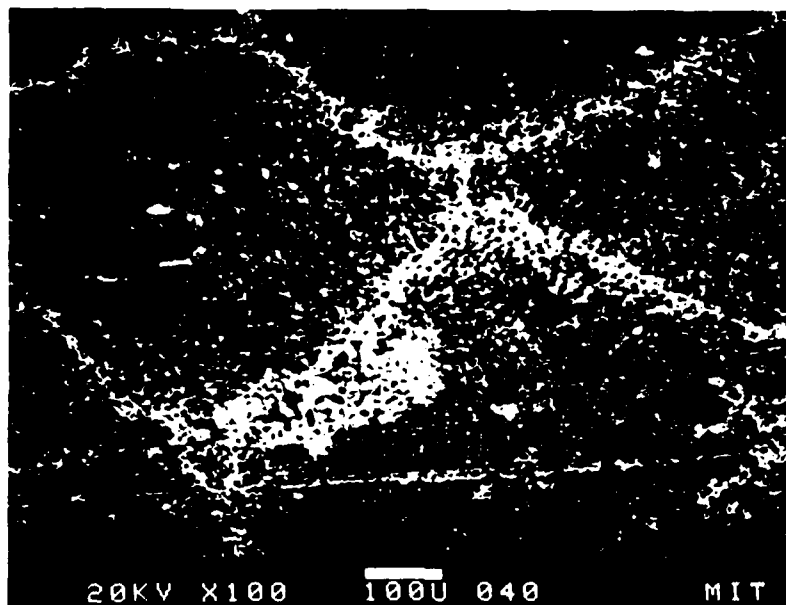


Figure 7: SEM micrograph showing the localized dissolution (induced by residual microstructural chloride) of the diffusion bond regions between precursor wires in a planar G/6061-T6 Al MMC six-ply plate electrode. The electrode was anodically polarized in deaerated 0.5 M  $\text{Na}_2\text{SO}_4$  of pH 7 at 30°C.

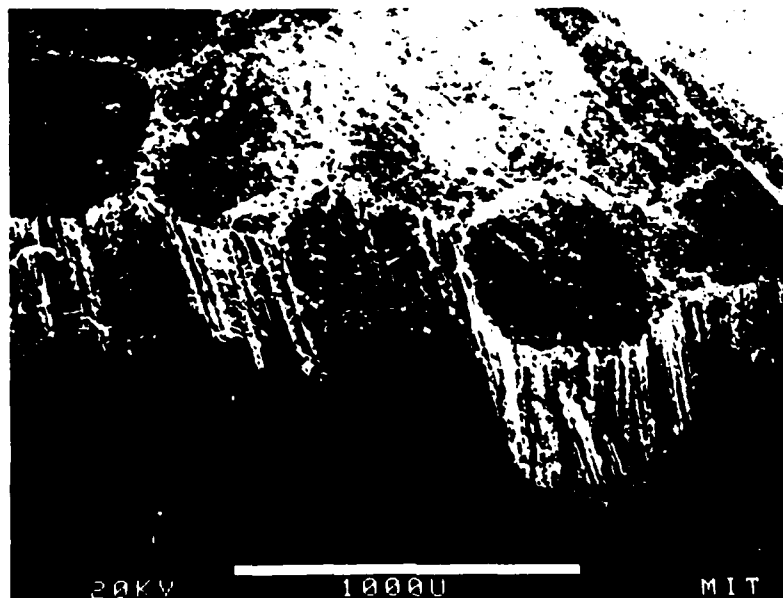


Figure 8: SEM micrograph of a planar G/6061-T6 Al MMC six-ply plate electrode showing the unbinding of precursor wires resulting from localized dissolution (induced by residual microstructural chloride) of the diffusion bond regions. The electrode was anodically polarized in deaerated 0.5 M  $\text{Na}_2\text{SO}_4$  of pH 7 at 30°C.

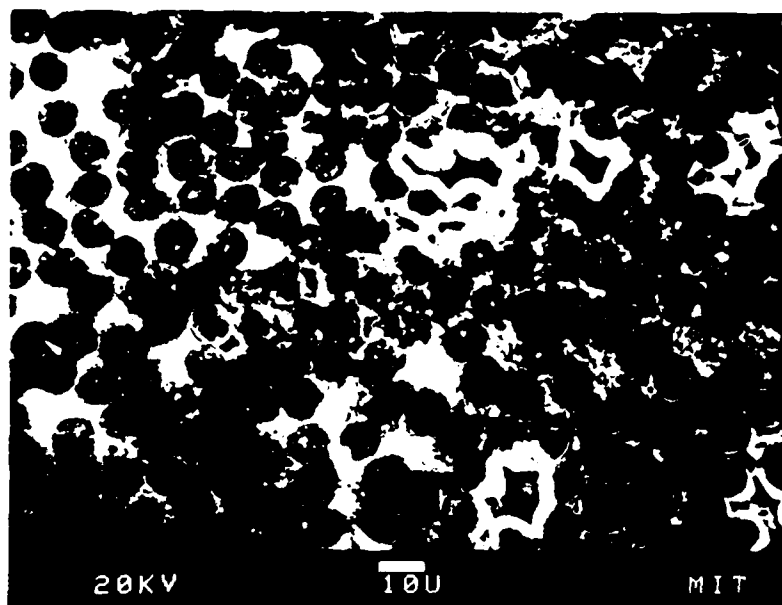


Figure 9: SEM micrograph of a planar G/6061-T6 Al MMC six-ply plate electrode showing localized dissolution (induced by residual microstructural chloride) in precursor interiors. Graphite fibers (dark) are in a 6061-T6 Al matrix (light). The electrode was anodically polarized in deaerated 0.5 M Na<sub>2</sub>SO<sub>4</sub> of pH 7 at 30°C.

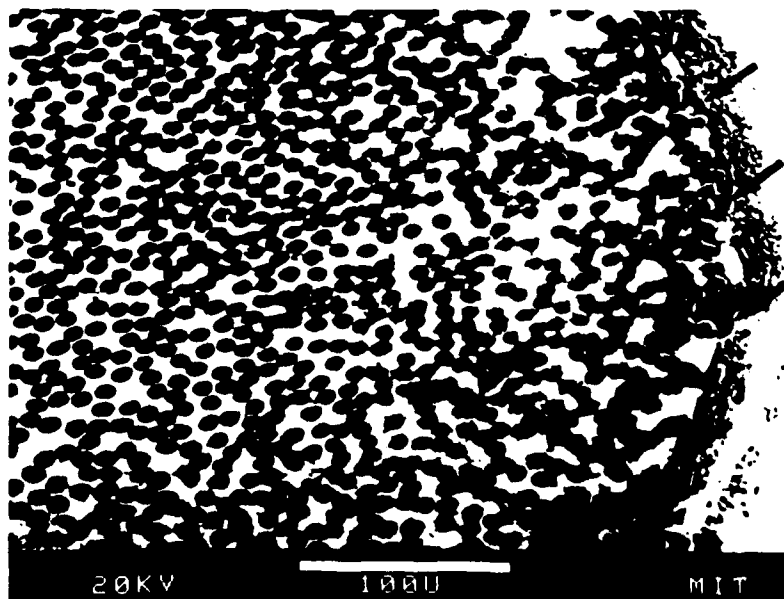


Figure 10: SEM micrograph showing localized dissolution (induced by residual microstructural chloride) in the perimeter region (indicated by arrows) of a planar G/6061-T6 Al MMC precursor wire electrode. The graphite fibers (dark) are in a 6061-T6 Al matrix (light). The precursor wire is mounted in epoxy. The electrode was anodically polarized in deaerated 0.5 M Na<sub>2</sub>SO<sub>4</sub> of pH 7 at 30°C.

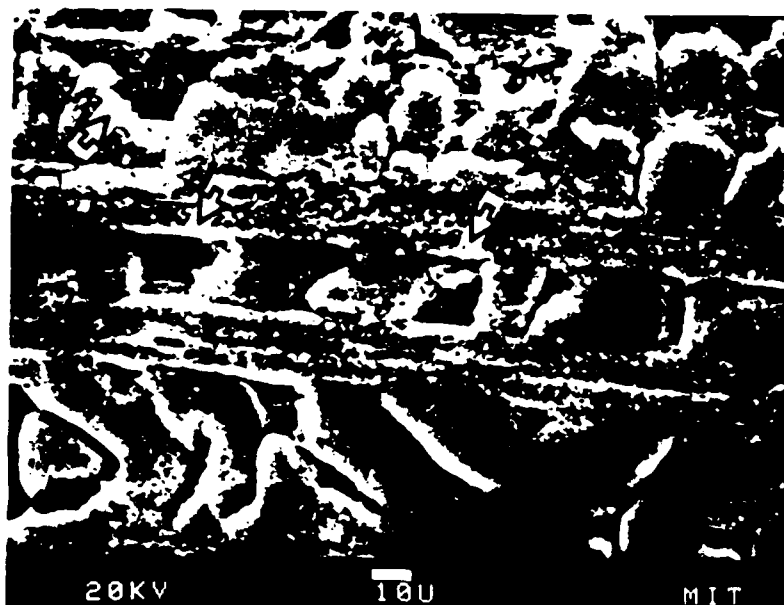


Figure 11: SEM micrograph showing pits (induced by residual microstructural chloride) in a precursor-wire skin electrode. The electrode was anodically polarized in deaerated 0.5 M  $\text{Na}_2\text{SO}_4$  of pH 7 at 30°C.

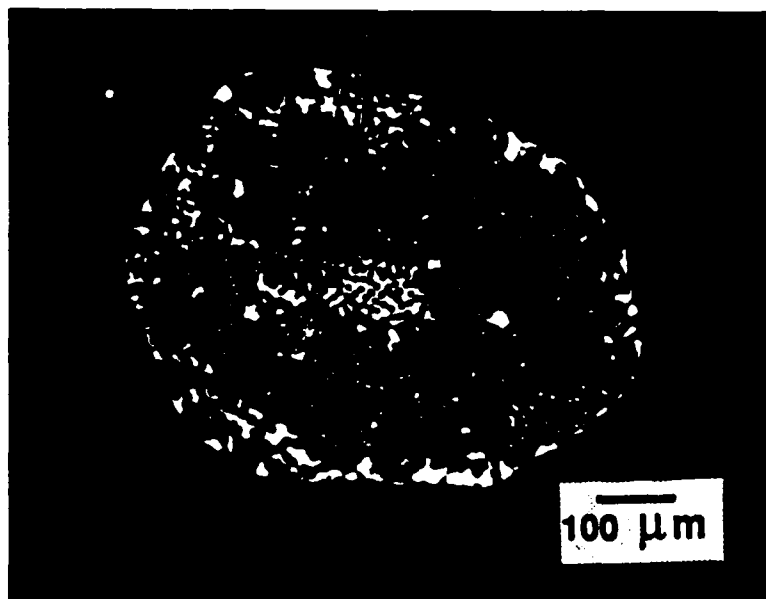


Figure 12: Cross section of the precursor-wire 6061-T6 Al skin electrode shown in Figure 11. The graphite fibers (dots) are perpendicular to the plane of the page. The bright regions are unconsumed 6061-T6 Al matrix. The electrode was anodically polarized in deaerated 0.5 M  $\text{Na}_2\text{SO}_4$  of pH 7 at 30°C.

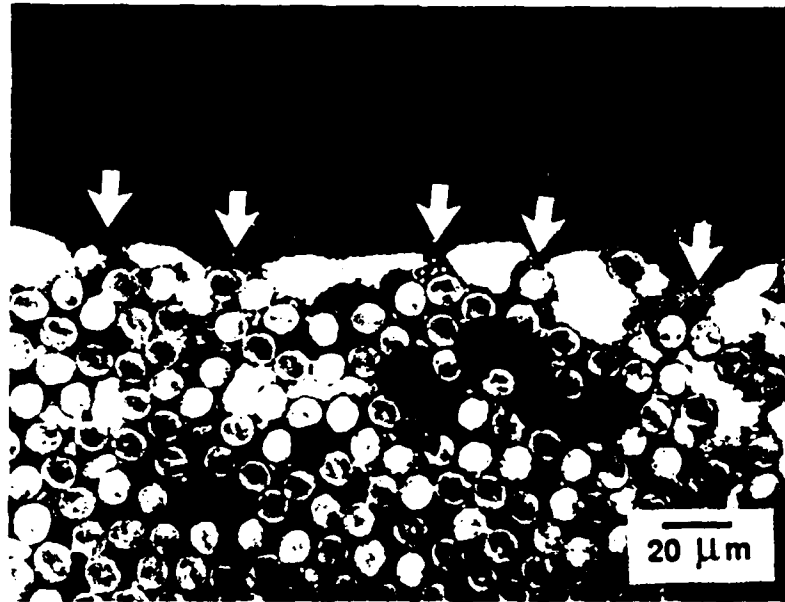


Figure 13: Enlarged view of Figure 12 showing sites where pits (indicated by arrows) initially penetrated the precursor-wire skin.



Figure 14: SEM micrograph showing crevices along the perimeters of graphite fibers in a planar G/6061-T6 Al MMC six-ply plate electrode that was anodically polarized at  $2.0 \text{ V}_{\text{SCE}}$  for 3.2 h in deaerated  $0.5 \text{ M Na}_2\text{SO}_4$  of pH 7 at  $30^\circ\text{C}$ . The formation of crevices was caused by  $\text{CO}_2$  evolution, resulting from the oxidation of graphite.

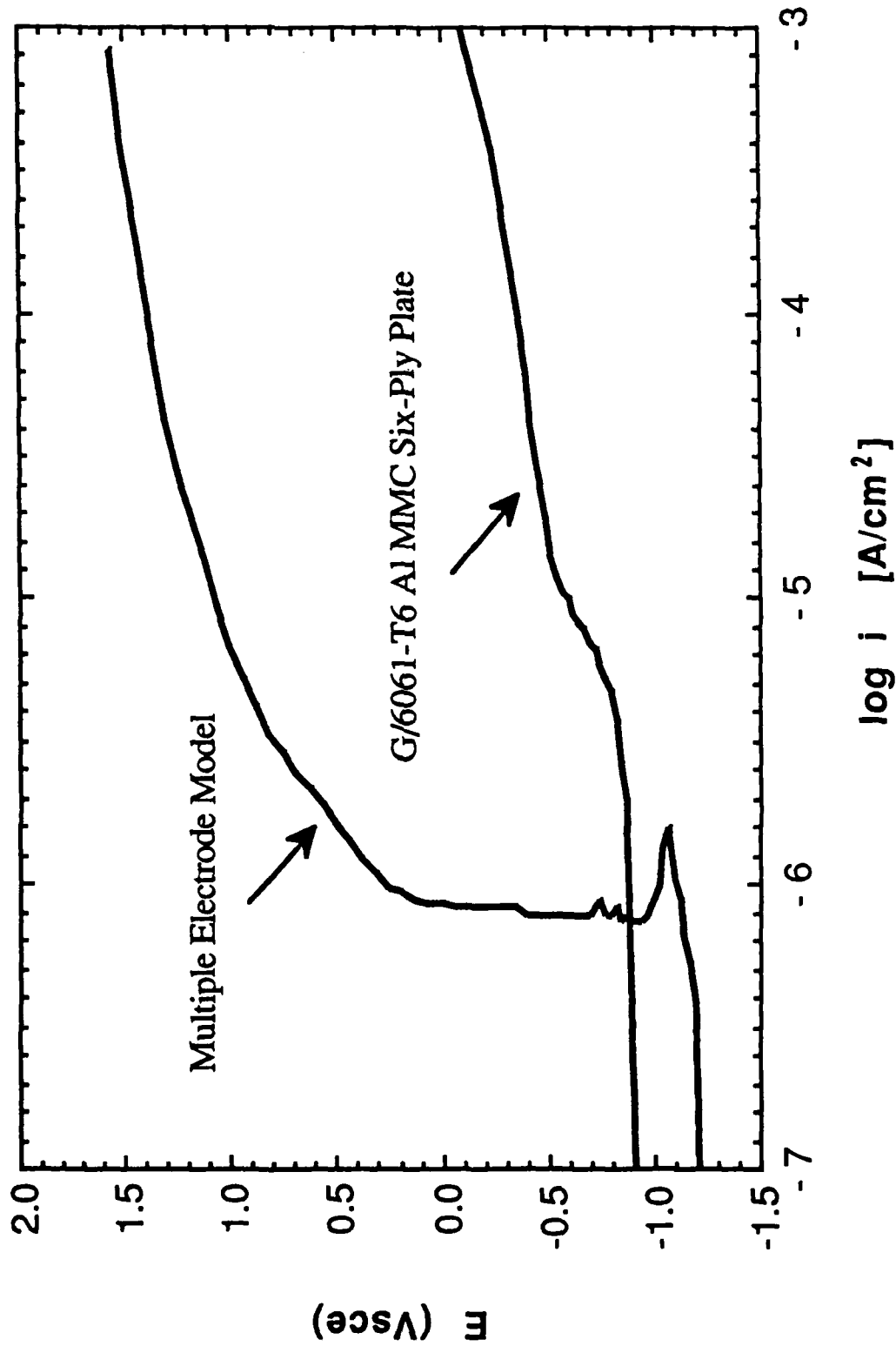


Figure 15: Comparison of the anodic polarization diagram of the multiple electrode model (consisting of 50% P100 graphite fiber and 6061-T6 Al) to that of the planar G/6061-T6 Al MMC ( $\approx$ 50 vol % P100 graphite) six-ply plate electrode exposed to deaerated 0.5 M  $Na_2SO_4$  of pH 7 at 30°C. Scan rate = 0.1 mV/s.

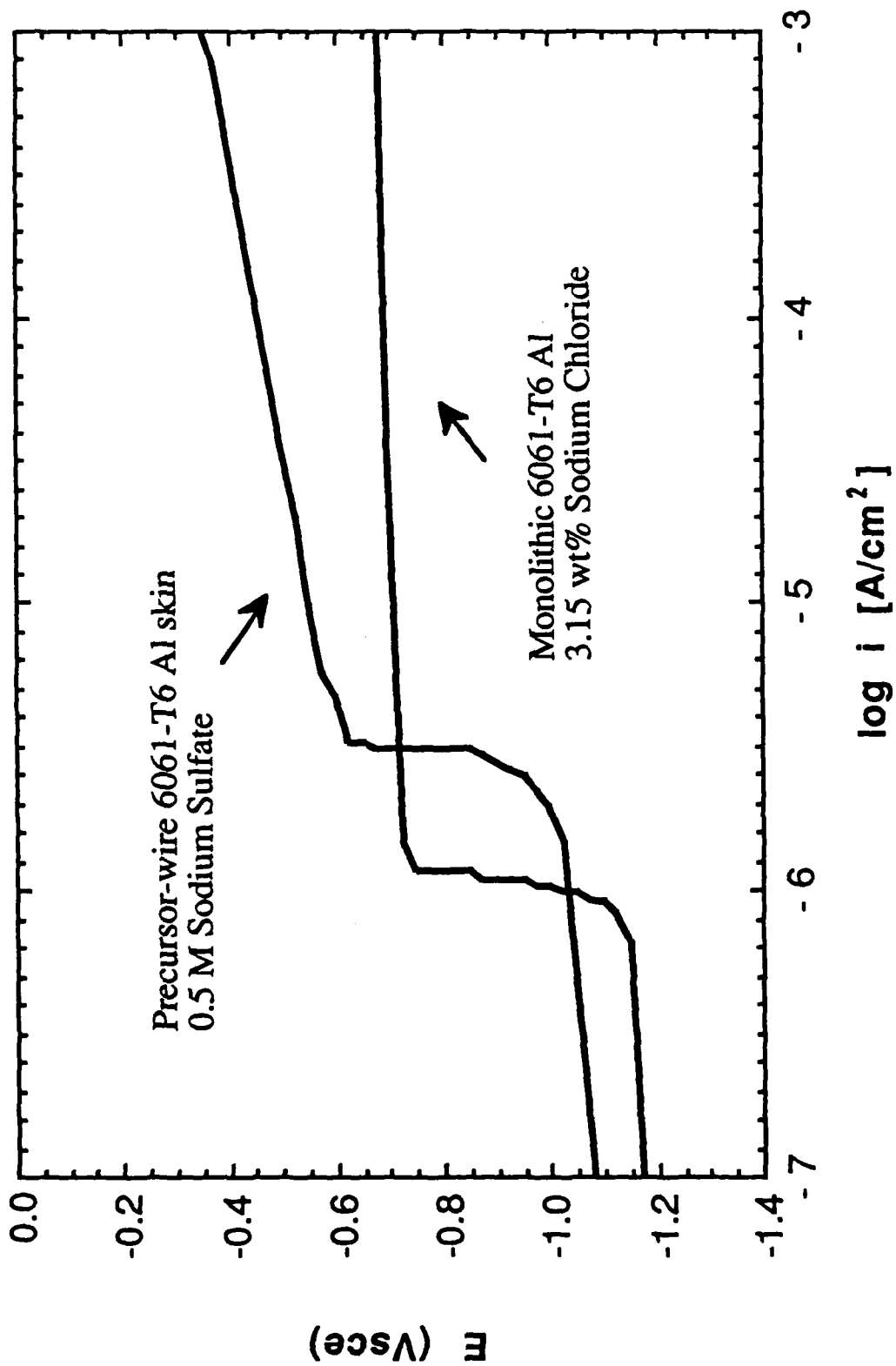


Figure 16: Comparison of the anodic polarization diagram of the precursor-wire 6061-T6 Al skin electrode exposed to deaerated chloride-free 0.5 M  $Na_2SO_4$  to that of monolithic 6061-T6 Al exposed to deaerated 3.15 wt% NaCl. Both solutions were of pH 7 at 30°C. Scan rate = 0.1 mV/s.

BASIC DISTRIBUTION LIST

Technical Reports and Publications

Feb 1990

<u>Organization</u>	<u>Copies</u>	<u>Organization</u>	<u>Copies</u>
Defense Documentation Center Cameron Station Alexandria, VA 22314	12	Naval Air Propulsion Center Trenton, NJ 08628 ATTN: Library	1
Office of Naval Research Dept. of the Navy 800 N. Quincy Street Arlington, VA 22217 ATTN: Code 1131	3	Naval Civil Engineering Laboratory Port Hueneme, CA 94043 ATTN: Materials Div.	1
Naval Research Laboratory Washington, DC 20375 ATTN: Codes 6000 6300 2627	1 1 1	Naval Electronics Laboratory San Diego, CA 92152 ATTN: Electronic Materials Sciences Division	1
Naval Air Development Center Code 606 Warminster, PA 18974 ATTN: Dr. J. DeLuccia	1	Commander David Taylor Research Center Bethesda, MD 20084	1
Commanding Officer Naval Surface Warfare Center Silver Spring, MD 20903-5000 ATTN: Library Code R33	1 1	Naval Underwater System Ctr. Newport, RI 02840 ATTN: Library	1
Naval Ocean Systems Center San Diego, CA 92152-5000 ATTN: Library	1	Naval Weapons Center China Lake, CA 93555 ATTN: Library	1
Naval Postgraduate School Monterey, CA 93940 ATTN: Mechanical Engineering Department	1	NASA Lewis Research Center 21000 Brookpark Road Cleveland, OH 44135 ATTN: Library	1
Naval Air Systems Command Washington, DC 20360 ATTN: Code 310A Code 5304B Code 931A	1 1 1	National Institute of Standards and Technology Gaithersburg, MD 20899 ATTN: Metallurgy Division Ceramics Division Fracture & Deformation Division	1 1 1
Naval Sea Systems Command Washington, DC 20362 ATTN: Code 05M Code 05R	1 1		

Naval Facilities Engineering Command Alexandria, VA 22331 ATTN: Code O3	1	Defense Metals & Ceramics Information Center Battelle Memorial Inst. 505 King Avenue Columbus, OH 43201	1
Commandant of the Marine Corps Scientific Advisor Washington, DC 20380 ATTN: Code AX	1	Oak Ridge National Laboratory Metals and Ceramics Div. P.O. Box X Oak Ridge, TN 37380 Oak Ridge, TN 37380	1 1
Army Research Office P.O. Box 12211 Research Triangle Park, NC 27709 ATTN: Metallurgy & Ceramics Program	1	Los Alamos Scientific Lab. P.O. Box 1663 Los Alamos, NM 87544 ATTN: Report Librarian	1
Army Materials Technology Laboratory Watertown, MA 02172-0001 ATTN: Research Program Office	1	Argonne National Laboratory Metallurgy Division P.O. Box 229 Lemont, IL 60439	1
Air Force Office of Scientific Research Building 410 Bolling Air Force Base Washington, DC 20332 ATTN: Electronics & Materials Science Directorate	1	Brookhaven National Laboratory Technical Information Division Upton, Long Island New York 11973 ATTN: Research Library	1
NASA Headquarters Washington, DC 20546 ATTN: Code RM	1	Lawrence Berkeley Lab. 1 Cyclotron Rd Berkeley, CA 94720 ATTN: Library	1
		David Taylor Research Ctr Annapolis, MD 21402-5067 ATTN: Code 281 Code 2813 Code 0115	1 1 1

RE/1131/88/75  
4315 (036)

Supplemental Distribution List

Feb 1990

Profs. G.H. Meier and F.S. Pettit  
Dept. of Metallurgical and  
Materials Eng.  
University of Pittsburgh  
Pittsburgh, PA 15261

Dr. G. D. Davis  
Martin Marietta Laboratories  
1450 South Rolling Rd.  
Baltimore, MD 21227-3898

Prof. H.K. Birnbaum  
Dept. of Metallurgy & Mining Eng.  
University of Illinois  
Urbana, Ill 61801

Prof. P.J. Moran  
Dept. of Materials Science & Eng.  
The Johns Hopkins University  
Baltimore, MD 21218

Prof. H.W. Pickering  
Dept. of Materials Science and Eng.  
The Pennsylvania State University  
University Park, PA 16802

Prof. J. Kruger  
Dept. of Materials Science & Eng.  
The Johns Hopkins University  
Baltimore, MD 21218

Prof. D.J. Duquette  
Dept. of Metallurgical Eng.  
Rensselaer Polytechnic Inst.  
Troy, NY 12181

Dr. B.G. Pound  
SRI International  
333 Ravenswood Ave.  
Menlo Park, CA 94025

Prof. D. Tomanek  
Michigan State University  
Dept. of Physics and Astronomy  
East Lansing, MI 48824-1116

Prof. C.R. Clayton  
Department of Materials Science  
& Engineering  
State University of New York  
Stony Brook  
Long Island, NY 11794

Dr. M. W. Kendig  
Rockwell International Science Center  
1049 Camino Dos Rios  
P.O. Box 1085  
Thousand Oaks, CA 91360

Dr. J. W. Oldfield  
Cortest Laboratories Ltd  
23 Shepherd Street  
Sheffield, S3 7BA, England

Prof. R. A. Rapp  
Dept. of Metallurgical Eng.  
The Ohio State University  
116 West 19th Avenue  
Columbus, OH 43210-1179

Prof. Boris D. Cahan  
Dept. of Chemistry  
Case Western Reserve Univ.  
Cleveland, Ohio 44106

Dr. R. W. Drisko  
Code L-52  
Naval Civil Engineering Laboratory  
Port Hueneme, CA 93043-5003

Prof. G. Simkovich  
Dept. of Materials Science & Eng.  
The Pennsylvania State University  
University Park, PA 16802

Dr. R.D. Granata  
Zettlemoyer Center for Surface Studies  
Sinclair Laboratory, Bld. No. 7  
Lehigh University  
Bethlehem, PA 18015

Prof. M.E. Orazem  
Dept. of Chemical Engineering  
University of Florida  
Gainesville, FL 32611